PHYSICAL REVIEW E **82**, 051907 (2010)

Queueing induced by bidirectional motor motion near the end of a microtubule

Peter Ashwin,[1] Congping Lin,[1,2] and Gero Steinberg[2]
[1]*Mathematics Research Institute, University of Exeter, Exeter, Devon EX4 4QF, United Kingdom*
[2]*School of Biosciences, University of Exeter, Exeter, Devon EX4 4QD, United Kingdom*
(Received 13 August 2010; published 4 November 2010)

Recent live observations of motors in long-range microtubule (MT) dependent transport in the fungus *Ustilago maydis* have reported bidirectional motion of dynein and an accumulation of the motors at the polymerization-active (the plus-end) of the microtubule. Quantitative data derived from *in vivo* observation of dynein has enabled us to develop an accurate, quantitatively-valid asymmetric simple exclusion process (ASEP) model that describes the coordinated motion of anterograde and retrograde motors sharing a single oriented microtubule. We give approximate expressions for the size and distribution of the accumulation, and discuss queueing properties for motors entering this accumulation. We show for this ASEP model, that the mean accumulation can be modeled as an $M/M/\infty$ queue that is Poisson distributed with mean F_{arr}/p_d, where F_{arr} is the flux of motors that arrives at the tip and p_d is the rate at which individual motors change direction from anterograde to retrograde motion. Deviations from this can in principle be used to gain information about other processes at work in the accumulation. Furthermore, our work is a significant step toward a mathematical description of the complex interactions of motors in cellular long-range transport of organelles.

DOI: 10.1103/PhysRevE.82.051907 PACS number(s): 87.16.Wd, 05.70.Ln, 72.20.Ee

I. INTRODUCTION

Cells are dynamic entities that maintain their organization by active transport of organelles and vesicles along the fibers of the cytoskeleton; the molecular machines driving this intracellular transport are known as molecular motors. Long-range organelle motility requires microtubules and the associated molecular motors kinesin and dynein. Kinesin takes its cargo to the polymerization-active plus-end of the microtubule (MT), whereas dynein "walks" toward minus-ends [1]. Much is known about the motility behavior of purified motors *in vitro*. Motility parameters, such as attachment and detachment rates or velocities have been measured in these *in vitro* assays. Based on this knowledge, numerous modeling approaches have attempted to describe the behavior of the counteracting motors kinesin and dynein. Indeed, mathematical modeling has revealed new concepts of motor coordination [2,3]. These theoretical approaches have significantly helped biologists to understand motor behavior in the living cell [4].

Most information on molecular motor behavior has hitherto been based on *in vitro* assays using purified proteins and often nonphysiological conditions. While the limited availability of consistent data makes assumptions necessary, the observed variation of the measured motor parameters is remarkable and raises some doubt about the accuracy of such models. One example is the amount of force that can be exerted by kinesin-3, which was found to be 5–6 pN for Dictyostelium discoideum kinesin-3 [5] but only 0.15 pN for single kinesin-3 motors from mammalian neurons [6]. Furthermore, it is likely that attachment rates and detachment rates of motors to MTs depend on additional microtubule-associated proteins [7,8], that motor run-length can be limited by obstacles along the track [9,10] and that it depends on associated factors that we are just beginning to understand [8,11]. Finally, modeling often builds on information about motors derived from different experiments using various motors from different cell types. However, motors can be visualized in living cells [12–14], raising the possibility that mathematical models can be built on quantitative descriptions of motor behavior in living cells. Recent live cell imaging approaches using a fungal model system have helped to overcome some of these experimental limitations. Visualization of native levels of molecular motors in living cells provides robust quantitative data for motor behavior in long-range motility *in vivo* [15].

The main contribution of this paper is to examine a model with appropriate boundary conditions that allows us to predict accumulation sizes on the basis of measurable parameters in such a system. We are motivated by a particular example of coordinated motor processes for transport within the fungus pathogen *Ustilago maydis* as observed by [15] on single oriented MTs at the tip of growing hyphae. We make use of data in that paper to develop a novel mathematical model. Due to the fact that our model is almost exclusively based on quantitative data derived from the *in vivo* observation of one cell type, we were able to develop a model of high accuracy that allows predictions that can be experimentally tested. We approximate the model by examining the steady state occupation of sites at the tip of a MT and making a mean field approximation.

The paper is organized as follows: in Sec. II we review models of bidirectional motility and introduce a stochastic exclusion model for bidirectional motion. In Sec. III we analyze the equilibrium distributions of the model using mean-field approximations. This is used to perform quantitative estimates of the size of the accumulation at the tip in Sec. IV. Finally, in Sec. V we discuss predicted queueing properties of motors in the tip. Few authors have explicitly considered queueing properties of motors (Arita [16] is an exception) and we suggest that precise measurements of queueing properties will in future be an important way to test models and to gain a better understanding of the within-cell transport processes.

II. MODELING BIDIRECTIONAL MOTOR MOTION

In [17] Reichenbach *et al.* (motivated by spin systems) consider the motion of two species along parallel tracks with an assumption that they can hop between the two tracks with a certain probability. They find that this can increase the propensity of the system to form blockages. Hough *et al.* [18] introduce and discuss a mathematical model of motor crowding that appears during motor-catalyzed depolymerization of MTs. Other models of transport include the possibility of "blockages" of motors using two species of motors that move in opposite directions (kinesins and dyneins) as detailed in [19]. The model they consider consists of two species of motors (dynein and kinesin) that move on a single MT, but may detach and enter a diffusive phase. They find clusters formed by motors moving in opposite directions, forming stationary blockages on a single MT filament. In [20] the authors note that the former models may be "unrealistically inefficient due to jam formation" and propose possible solutions to this problem by modifying the dynamics of the network. In another approach to bidirectional transport on a single track, Lui *et al.* [21] consider a system where exclusion only applies to motors moving in the same direction; the presence of a motor in the opposite direction modifies the rate at which motors can enter the site.

Our approach is closest to a model of Juhász [22,23], who considers a system where indistinguishable particles are transported in to the right on one lane (say A) and to the left on a second (say B), and where particles can switch lanes at a certain rate. This in principle permits much larger fluxes of motors in both directions than observed in [19] as the motions in each direction are separated from collision. As molecular motors only perform unidirectional motion on an oriented MT, this model poses the question as to how one can use the model to understand the coordination of real *in vivo* transport processes unless one interprets the two lanes A and B as being an antiparallel arrangement of microtubules.

Nonetheless, recent experiments suggest that head-on collisions of kinesin and dynein on a single microtubule are rare and, at least away from any buildups of motors, we can interpret the lanes of [22] as independent bidirectional motion of the motors; the switching of lanes simply corresponds to dynein moving from active retrograde to passive anterograde transport. Because of this, we interpret the ASEP process of [22] as modeling a coordinated bidirectional motion of individual dynein motors on a single MT. Although [22] only considers one species of motor that moves in antiparallel lanes, we interpret this as motion on a single MT in the following way: We assume that dynein move under their own power in one direction, but they are carried by kinesin-1 bound to the dynein while moving in the other direction. The entire motion is assumed to take place on a single MT.

A. Assumptions for the model

Consider an oriented MT aligned from left (minus end) to right (plus end) parametrized by a spatial variable x. There are typically several populations of motors that may use a single MT *in vivo*, and in this model we concentrate on one of these; a dynein that moves to the minus end when bound to a MT, but which can be carried as a cargo of a kinesin to the plus end. We assume

(H1) All motors are one of two types-moving either to the right or to the left.

(H2) Right and left moving motors pass without interaction, but there is an "exclusion principle" that means a motor can only move forward if the site ahead is free of motors of the same type.

(H3) In the dilute state, the motors move at a mean velocity v_+ and v_- to the right/left, respectively.

(H4) There is a random switching of direction where right-moving motors change to left-moving at a rate p_d, and left-moving motors change to right-moving at a rate p_u, where $p_{d,u}$ can be expressed by velocities and $M_{a,r}$, the mean free run length of left (right) moving motors before turning as $p_d=v_+/M_a$ ($p_u=v_-/M_r$).

We are particularly interested in the boundary conditions inferred from these experiments for a single MT at the hyphal tip of the fungus *Ustilago maydis* [15]. For this reason we assume

(H5) The right boundary of the MT has no-flux boundary conditions.

(H6) The right-moving motors appear at the left boundary with flux rate $\alpha_+=F_{in}$ while left-moving motors exit without impediment.

Finally we assume

(H7) The system is in statistical equilibrium.

This suggests an ASEP model with two lanes; assumptions H1–H4 are essentially the same as considered by Juhász [23], though we consider different boundary conditions (H5–H7). In that paper right moving motors exit without impediment, while here they cannot exit. The effect of this is that the predictions in [23] on net flux rates is not applicable here; assumptions H5–H7 imply that the net flux must be zero. Table I gives measured or estimated values for the parameters discussed.

TABLE I. Parameters used in the simulations. The values for $v_\pm$, $M_a=v_+/p_d$, $M_r=v_-/p_u$, and F_{in} are from *in vivo* experiments on *Ustilago maydis* (see [15]). The space step h corresponds to the size of the monomers making up the MT and is taken from [24]. The length L of the simulation corresponds to the field of view used for the kymographs.

v_+	Velocity to right	1.66 μm s^{-1}
v_-	Velocity to left	1.76 μm s^{-1}
M_a	Mean anterograde run-length	41.89 μm
M_r	Mean retrograde run-length	62.37 μm
F_{in}	Flux of anterograde dynein at a distance L from tip	1.06 s^{-1}
h	Space step	8 nm
L	Length of simulation	10 μm

B. Discrete model for bidirectional coordinated motor motion

We discretize the single MT into two notional tracks; one for motors (dynein carried by kinesin-1) going toward the plus-end, and one for motors (dynein) going toward the

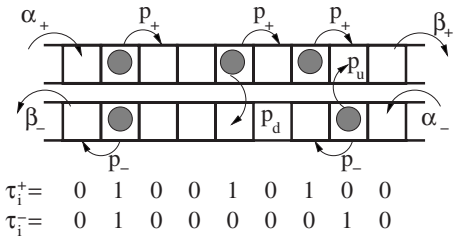

FIG. 1. Schematic diagram of the states and transition rates for the ASEP approximating bidirectional motion of the particles representing motors. The "plus-end" of the MT is on the right, and each track has dynein motors (represented as filled disks) moving in only one direction, carried to the right by kinesin-1 on the upper track, and moving to the left under their own power on the lower track. The motors move as shown with rates p_+, p_-. The change direction with rate p_d (down to the left moving track) or p_u (up to the right moving track). Motors are injected into the +/− tracks at rate $\alpha_\pm$ and leave at rate $\beta_\pm$ as shown.

minus-end. On each track we assume there are sites separated by steps of length h; we refer to a "site" as an adjacent location on both tracks; this is illustrated in Fig. 1. Let $\tau_i^\pm$ represent the state of the system for $i=1,\cdots N$. The model updates this as time progresses to give $\tau_i^\pm(t)$; in the rightwards direction, $\tau_i^+=0$ if the site is empty and $\tau_i^+=1$ if it is occupied; similarly $\tau_i^-(t)$ encodes the motion of leftwards-moving motors (see Fig. 1).

We formulate a model using H1–H4 by assuming the following occur at given rates: occupants of + sites move one step to the right with rate p_+ if the site is empty (an exclusion principle) while occupants of the − sites move one step to the left with rate p_- subject to a similar exclusion principle. We assume that changes in direction from right-going to left-going occur with rate p_d while from left-going to right-going occur with rate p_u, with the obvious exclusion principles blocking the possibility of more than one particle at any site. The rates, in terms of H1–H4 and h can be written

$$p_+ = \frac{v_+}{h}, \quad p_- = \frac{v_-}{h}, \quad p_d = \frac{v_+}{M_a}, \quad p_u = \frac{v_-}{M_r}. \tag{1}$$

Figure 2 shows a comparison of an experimentally measured kymograph (a time-distance graph) showing the motion of photoactivated dynein moving on a single MT near a hyphal tip of *Ustilago maydis*, and a simulated kymograph using the model illustrated in Fig. 1 with parameters in Table I. The parameters for the simulation are obtained from experimental images such as Fig. 2 by measurement of the slopes of the observed kymograph traces (to give $v_\pm$), the frequency of turning of left- or right-going traces [to give $p_{u,d}$ and hence from Eq. (1) M_a and M_r] and the flux rates (to give the boundary conditions for the simulation). In [15], the turning rate is extracted by measuring the fraction of motors passing a fixed reference point that have traveled less than a given distance past this point before turning; this is fitted to an exponential distribution with mean distance M_a (respectively, M_r) and then Eq. (1) is used to give $p_{u,d}$. For more details of experimental measurement of the parameters see [15]. We note here that

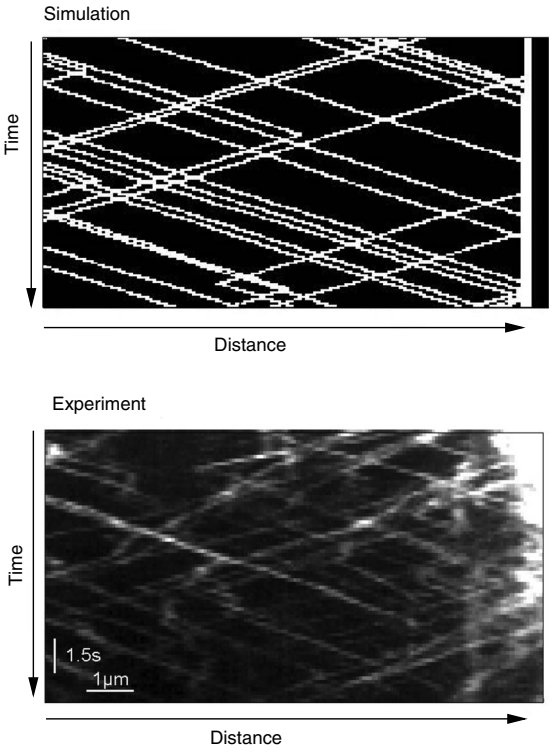

FIG. 2. Top: a simulated kymograph using the model in Fig. 1 and parameters in Table I. Bottom: an experimentally measured kymograph showing dynein motion over 10 μm near the hyphal tip of the fungus *Ustilago maydis*, obtained using methods described in [15]. Dynein moves away from the tip under its own power, and is carried by kinesin-1 toward the tip; it is visualized by fluorescent GFP attached to endogenous copies of the dynein. Observe (a) the presence of an accumulation of dynein on the right hand side in both cases, (b) the apparent absence of any significant interaction between counter-moving motors, (c) the occasional change in direction away from the tip and (d) the velocities (represented by the slopes in either direction) are consistent along the microtubule.

(a) From Table I, the two velocities $v_\pm$ are of similar magnitudes and individual motors are visible as they are relatively dilute on MT away from the end of the MT;

(b) The motors moving in opposite directions seem to pass each other with no measurable interaction, suggesting that the two-lane model is reasonable;

(c) The turning rates are small, meaning that the majority of motors move from one end of the MT and enter an accumulation that is at the plus-end of the MT; the mean free run-length is longer than the illustrated section of MT;

(d) Individual motors can be observed to enter the tip, remain there for some time and then leave. We will be concerned with estimating the *tip size*, i.e., the average number of motors that are queued at the tip at any one time.

III. MEAN-FIELD ANALYSIS OF EQUILIBRIUM STATES

The ASEP model in Fig. 1 is not amenable to explicit analytic solution and so we use a mean field approximation as in [23] to reduce the system to an approximating PDE. If we define

$$\rho_i = \langle \tau_i^+ \rangle, \quad \sigma_i = \langle \tau_i^- \rangle$$

to be the average occupancy of site i where the average is over an ensemble of initial states, then a mean field approximation assumes that occupancy properties of the adjacent sites are independent of each other. This gives the approximation

$$\frac{d\rho_i}{dt} = p_+\rho_{i-1}(1-\rho_i) - p_+\rho_i(1-\rho_{i+1}) - p_d\rho_i(1-\sigma_i) + p_u\sigma_i(1-\rho_i),$$

$$\frac{d\sigma_i}{dt} = p_-\sigma_{i+1}(1-\sigma_i) - p_-\sigma_i(1-\sigma_{i-1}) - p_u\sigma_i(1-\rho_i) + p_d\rho_i(1-\sigma_i). \tag{2}$$

We approximate this further to a partial differential equation by considering a spatial variable $x \in [0,1]$ and noting that if $x = i\delta$ where $\delta = h/L$ is a small parameter, then

$$\rho_{i\pm1} = \rho_i \pm \delta\frac{\partial\rho_i}{\partial x} + \frac{\delta^2}{2}\frac{\partial^2\rho_i}{\partial x^2} + O(\delta^3),$$

$$\sigma_{i\pm1} = \sigma_i \pm \delta\frac{\partial\sigma_i}{\partial x} + \frac{\delta^2}{2}\frac{\partial^2\sigma_i}{\partial x^2} + O(\delta^3),$$

where all derivatives are evaluated at x. Ignoring terms of order $O(\delta^2)$, Eq. (2) can be written as

$$\frac{\partial\rho}{\partial t} = -p_d\rho(1-\sigma) + p_u\sigma(1-\rho) + \frac{v_+}{L}(2\rho-1)\frac{\partial\rho}{\partial x} + \delta\frac{v_+}{2L}\frac{\partial^2\rho}{\partial x^2},$$

$$\frac{\partial\sigma}{\partial t} = p_d\rho(1-\sigma) - p_u\sigma(1-\rho) + \frac{v_-}{L}(1-2\sigma)\frac{\partial\rho}{\partial x} + \delta\frac{v_-}{2L}\frac{\partial^2\sigma}{\partial x^2}. \tag{3}$$

Adding these two equations gives

$$\frac{\partial(\rho+\sigma)}{\partial t} = \frac{\partial}{\partial x}\left[\frac{v_+}{L}(\rho^2-\rho) - \frac{v_-}{L}(\sigma^2-\sigma)\right] + \delta\left(\frac{v_+}{2L}\frac{\partial^2\rho}{\partial x^2} + \frac{v_-}{2L}\frac{\partial^2\sigma}{\partial x^2}\right) = \frac{\partial}{\partial x}J[\rho(x,t),\sigma(x,t)] \tag{4}$$

where

$$J(x,t) = \frac{v_+}{L}(\rho^2-\rho) - \frac{v_-}{L}(\sigma^2-\sigma) + \delta\left(\frac{v_+}{2L}\frac{\partial\rho}{\partial x} + \frac{v_-}{2L}\frac{\partial\sigma}{\partial x}\right).$$

Any stationary state will satisfy $\frac{\partial J}{\partial x}=0$ meaning that the steady-state net flux along the domain is constant independent of x. To first order in δ the steady-state satisfies

$$0 = -p_d\rho(1-\sigma) + p_u\sigma(1-\rho) + \frac{v_+}{L}(2\rho-1)\frac{d\rho}{dx},$$

$$0 = -p_u\sigma(1-\rho) + p_d\rho(1-\sigma) + \frac{v_-}{L}(1-2\sigma)\frac{d\sigma}{dx}. \tag{5}$$

Note that $\frac{v_\pm}{L}$ has units of s^{-1}. The net flux can be written in this case as

$$j_+(x) - j_-(x) = J_0. \tag{6}$$

The quantities $j_+(x)=\frac{v_+}{L}(\rho-\rho^2)$ and $j_-(x)=\frac{v_-}{L}(\sigma-\sigma^2)$ are the fluxes of the left and right-going particles. The mean field equations are well-known to have solutions with shock formation; the second derivative (diffusion) terms act as a singular perturbation that permits shocks or boundary layers to form between regions where Eq. (6) is a valid approximation.

Asymptotic form of the shock solution

Consider the mean-field model (3) on the spatial domain x in the interval [0,1] with boundary conditions as illustrated in Fig. 1. As described in [22] the equilibrium state may have boundary layers depending on the phase and the boundary conditions. General boundary conditions $\alpha_\pm$ and $\beta_\pm$ for the mean field model (3) on a spatial domain $x \in [0,1]$ may be replace by *effective boundary conditions* that will depend on the phase induced within the system; for example an effective boundary condition $\alpha_{+,\mathrm{eff}}=\min(\alpha_+,p_+/2)$ recognizes that no injection rate can induce more than a maximal current.

The symmetric cases $\alpha=\alpha_+=\alpha_-$ and $\beta=\beta_+=\beta_-$ together with $p_+=p_-=1$ are discussed in [22], while [23] examines the case $\alpha_-=0$ and $\beta_+>0$. In this paper, we consider the case of the plus end blocked, i.e., $\alpha_-=\beta_+=0$ so that the balanced total flux J_0 is zero and a boundary layer may develop on one (or both) of the left-hand boundaries.

We concentrate on the case of injection and escape at $x=0$ (α_+/p_+ small, $\beta_-=p_-$) and no-flux at $x=1$: ($\alpha_-=0$, $\beta_+=0$). This can be expressed as boundary conditions on the densities,

$$\rho(0) = \frac{\alpha_+}{p_+} = \delta\frac{F_{in}L}{v_+}, \quad \sigma(0) = 0,$$

$$\rho(1) = 1, \quad \sigma(1) = 0,$$

where a boundary layer will appear in $\sigma(x)$ at $x=0$; we can remove this by replacing this boundary condition with an effective boundary condition, solving Eq. (10) to give $\sigma(0)$ in terms of $\rho(0)$. Note that both fluxes at the right are zero, meaning that the net flux is zero.

In the case where $v=v_+=v_-$ we can solve $J_0=0$ in Eq. (6) to give

$$\rho = \sigma, \quad \text{or} \quad \rho = 1-\sigma. \tag{7}$$

These states are termed *equal-density* and *complementary-density*, respectively, in [22]. For *equal-density* states we have

$$0 = \frac{v}{L}(2\rho-1)\frac{d\rho}{dx} + (p_u-p_d)\rho(1-\rho)$$

so that

$$\rho(x) = \frac{1 \pm \sqrt{1 - 4C_e \exp[(p_u - p_d)xL/v]}}{2}, \tag{8}$$

where C_e is a constant. Similarly, for the *complementary-density* states we have

$$0 = \frac{v}{L}(2\rho - 1)\frac{d\rho}{dx} + p_u(1-\rho)^2 - p_d\rho^2, \tag{9}$$

which can in principle be integrated to give an implicit expression for the complementary-density states.

For a more general case of v_+ and v_- shocks may also form in the system that join regions of equal density to those with complementary density [22,23]. As in [22], we classify the equilibrium state as H (high density) or L (low density) in each lane. For the parameters considered here, the system will be in a state where there is a shock from a LL state to a HL state; the shock corresponds to a change from equal density to complementary density. If we assume that there is a shock at $x=x_s \in (0,1)$ and write the densities

$$\rho(x) = \begin{cases} \rho_l(x) & \text{for } x < x_s \\ \rho_r(x) & \text{for } x > x_s \end{cases},$$

$$\sigma(x) = \begin{cases} \sigma_l(x) & \text{for } x < x_s \\ \sigma_r(x) & \text{for } x > x_s, \end{cases},$$

where $\rho_{l,r}$ ($\sigma_{l,r}$) are the solutions from left and right boundary for ρ (σ), then the fluxes in each direction will match across the shock

$$\lim_{x\to x_0^-} j_+(x) = \lim_{x\to x_0^+} j_+(x),$$

$$\lim_{x\to x_0^-} j_-(x) = \lim_{x\to x_0^+} j_-(x).$$

This matching implies $\rho_l(x_s) = 1 - \rho_r(x_s)$ or $\sigma_l(x_s) = \sigma_r(x_s)$. Section IV extends this analysis to the more general case of unequal velocities in retrograde and anterograde directions.

IV. QUANTITATIVE ESTIMATES FOR QUEUE SIZE

We assume that the flux F_{in} rate is small and accords with the *in vivo* experimental observations of [15]. In such a case there will be an equilibrium state where $\rho(x)$ and $\sigma(x)$ are approximately equal density from the left boundary up to a point close to the right boundary. At this "shock" there is a rapid transition to a region where the total density is almost full—a queue at the plus-end tip.

We will estimate the densities and tip size (the mean size of the motor accumulation at the plus-end) using simulations and analytical approximations of the model. We will be interested in properties of solutions where v_+ and v_- are

$$v_\pm = v(1 \pm \epsilon)$$

with v is the mean of the average velocity of motors in either direction and a small parameter ϵ. From the boundary conditions $\alpha_- = \beta_+ = 0$, the net flux must be zero ($J_0 = 0$), so that

$$\frac{\sigma^2 - \sigma}{\rho^2 - \rho} = \frac{1+\epsilon}{1-\epsilon}, \tag{10}$$

and hence

$$\sigma = \frac{1}{2}\left(1 \pm \sqrt{1 + 4\left(1 + \frac{2\epsilon}{1-\epsilon}\right)(\rho^2 - \rho)}\right).$$

We make the ansatz that there is a solution such that

$$\min[\rho(x), 1-\rho(x)] < K\delta,$$

$$\min[\sigma(x), 1-\sigma(x)] < K\delta \tag{11}$$

for small enough δ and seek a solution that satisfies this away from any shocks. Solving Eq. (10) with this ansatz gives a perturbed *equal-density* state

$$\sigma = \rho + \frac{2\epsilon}{1-\epsilon}\left[\frac{\rho^2 - \rho}{2\rho - 1}\right] + O(\delta^2) \tag{12}$$

and a perturbed *complementary-density* state

$$\sigma = 1 - \rho - \frac{2\epsilon}{1-\epsilon}\left[\frac{\rho^2 - \rho}{2\rho - 1}\right] + O(\delta^2). \tag{13}$$

For δ small, the inflowing boundary condition at $x=0$, $\rho(0) = \delta L F_{in}/v_+$, and a shock appears at $x_s = 1 - y \in (0,1)$ where

$$y = \delta n_{tip} + O(\delta^2).$$

This shock is a transition from LL to HL as described above and n_{tip} is the number of occupied sites at the tip and we refer to as the queue or tip size. In the equal density (LL) region $x \in (0, x_s)$ we have

$$0 = \frac{v_+}{L}(2\rho - 1)\frac{d\rho}{dx} + p_u\sigma(1-\rho) - p_d\rho(1-\sigma) + O(\delta^2).$$

Using the ansatz (11), noting that when $\frac{d\rho}{dx}$ and $\frac{d\sigma}{dx}$ are of order δ, and taking leading order terms we have

$$\frac{d\rho}{dx} = \frac{L}{v(1+\epsilon)}\left[\left(1 + \frac{2\epsilon}{1-\epsilon}\right)p_u - p_d\right]\rho$$

and so, using $v_+ = (1+\epsilon)v$ and the boundary condition $\rho_l(0) = F_{in}h/v_+$ we have

$$\rho_l(x) = \delta\frac{F_{in}L}{v_+}\exp\left[x\left(\frac{L}{M_r} - \frac{L}{M_a}\right)\right] + O(\delta^2)$$

when $x \in (0, x_s)$. In the complementary density region (HL) $x \in (x_s, 1)$ we have

$$\frac{v_+(2\rho-1)}{L}\frac{d\rho}{dx} = -p_u(1-\rho)\left(1 - \rho - \frac{2\epsilon}{1-\epsilon}\frac{\rho^2-\rho}{2\rho-1}\right) + p_d\rho\left(\rho + \frac{2\epsilon}{1-\epsilon}\frac{\rho^2-\rho}{2\rho-1}\right) + O(\delta^2)$$

so that to leading order we have $\frac{v_+}{p_d L}\frac{d\rho}{dx} = 1$. Applying the boundary condition $\rho(1) = 1$, we have

$$\rho_r(x) = 1 + \frac{p_d L}{v_+}(x-1) + O(\delta^2).$$

Balancing the flux on the right-moving track at the shock $x = x_s = 1 - \delta n_{tip} + O(\delta^2)$ allows us to find a solution that satisfies the ansatz (11). For n_{tip} large this will give a solution

with a shock of width approximately 2δ from Eq. (6) and a boundary layer if n_{tip} is small. From $\rho_l(x_s)=1-\rho_r(x_s)$, we take the first order in δ, leading to

$$\delta n_{tip} L \frac{p_d}{v_+} \approx \delta \frac{F_{in} L}{v_+} \exp\left(\frac{L}{M_r} - \frac{L}{M_a}\right),$$

which means that the average number of motors at the tip is

$$n_{tip} \approx \frac{F_{in}}{p_d} \exp\left(\frac{L}{M_r} - \frac{L}{M_a}\right), \tag{14}$$

where $p_d = \frac{v_+}{M_a}$.

Denoting by F_{arr} the leading order flux of arrivals at the tip of the MT, to leading order $F_{arr}=F_{in}\exp(\frac{L}{M_r}-\frac{L}{M_a})$, meaning that we can express the leading order mean tip size as

$$n_{tip} \approx \frac{F_{arr}}{p_d}. \tag{15}$$

Tip size from simulations

To confirm the results in the previous section, we have performed stochastic simulations using both Gillespie and parallel update Monte Carlo algorithms. The Gillespie algorithm [25] produces quantitatively correct statistics for events that are instantaneous and independently distributed in an exponential manner. We use a small enough time step ($h_t=4.2\times10^{-3}$ s) to resolve the fastest process at each site in a Monte Carlo simulation. The sequence of updates may affect the outcome, so we specify that we update first the anterograde lane and then the retrograde lane. For both Gillespie and Monte Carlo schemes we use simulation time of at least order $t=160$ s, taking care to ensure that the system has reached a statistically stationary state before measuring tip size. There is no unique way to determine exactly where the queue for the tip starts—here we consider the following two definitions which agree well with a number of other definitions of tip size (not shown):

(a) We define n^d_{tip} to be the tip size as the total number of sites where the average density is over half where plus-direct current reaches its maximal, similar to the tip size definition in [26].

(b) We define n^s_{tip} to be the total sites that are occupied in an arbitrarily chosen "tip region" (in our case, the last 1 μm of the MT).

The quantity n^s_{tip} corresponds to the definition of tip size used in simulations in [15]. Using the measured parameters from [15] as in Table I, long simulations show that there is little difference in tip size between the two simulation algorithms: we find $n^d_{tip}=25$, $n^s_{tip}=25.4\pm0.22$ using the Monte Carlo and $n^d_{tip}=24$, $n^s_{tip}=25.3\pm0.29$ using the Gillespie algorithm. The explicit expressions (13) and (12) for the motor density ρ and σ are in good agreement with Gillespie and Monte Carlo simulations of the process as illustrated in Fig. 3; tip size for general velocity from analytical expression (14) is also in good agreement with simulation as illustrated in Fig. 4.

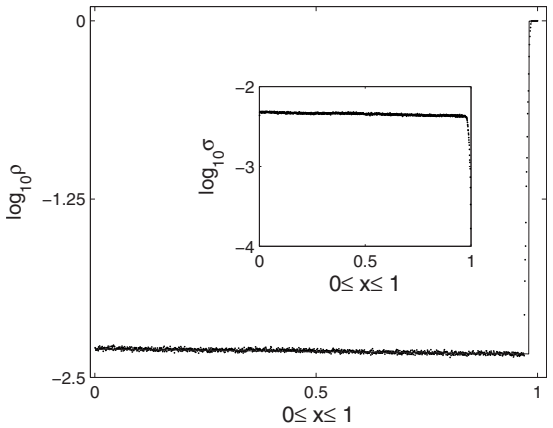

FIG. 3. A comparison of the mean field approximation of the densities ρ and σ from Eq. (12) to Eq. (13) (lines), with densities obtained from numerical simulations using a Monte Carlo algorithm (points). Parameters are as in Table I.

V. QUEUEING MODELS AT THE TIP

A. Queueing at the tip as an $M/M/\infty$-process

The motors that reach the tip for the ASEP model can be thought of as joining a queue that has approximately $M/M/\infty$ type—motors arrive at and leave from the tip with exponential (memoryless=M) distributions, and there is no limit in the number (∞) of identical "servers" at which a single motor can queue [27]. In our case, the arrival rate is F_{arr} while the leaving rate from each server is p_d.

This allows us to conceptually understand the queueing process at the tip as a quantitative process without worrying about detailed motion within the tip. Let $X(t)$ be the number of motors at the tip. In the stationary state, the mean tip size is simply the mean queue size [28],

$$\lim_{t\to\infty} E[X(t)] = F_{arr} E[M_1] = \frac{F_{arr}}{p_d},$$

where M_n is a random variable that gives the time spent by nth motor in the queue before it leaves; and $E[M_n]=1/p_d$.

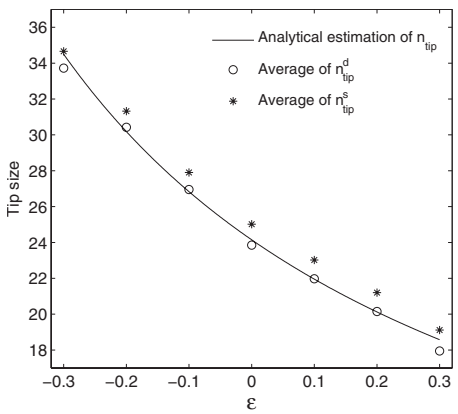

FIG. 4. Comparison of tip size predictions between simulation and analytical approximation from Eq. (14) for a range of unequal velocities parameterized by ϵ: parameters as in Table I except for $v_\pm=v(1\pm\epsilon)$ and $v=1.7$ μs^{-1}.

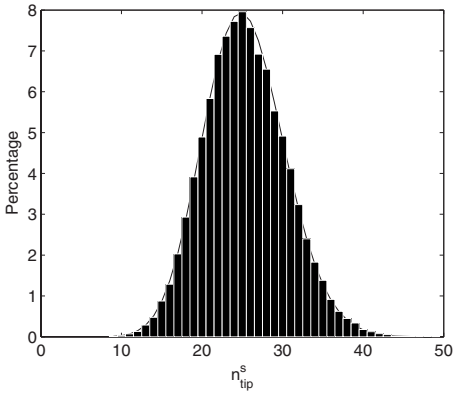

FIG. 5. The bar-graph shows the distribution of instantaneous tip size n^s_{tip} for parameters as in Table I. This was obtained using a Monte Carlo simulation with a very long sample length (2.1×10^5 s). The smooth curve shows a fit to a Poisson distribution with mean 25.3.

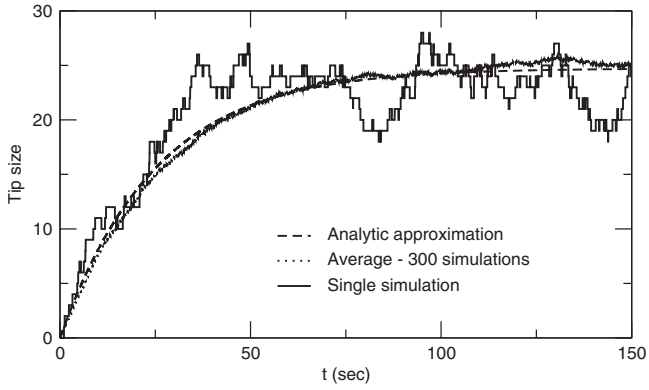

FIG. 6. Tip size as a function of time, starting from no motors at the tip, comparing the analytic approximation (17) with stochastic simulations using a Gillespie algorithm. The ensemble average over 300 simulations (parameters as in Table I) and a single simulation are shown.

We write the distribution of tip sizes at time t as $Q_n(t)=P[X(t)=n]$. Assuming that a flux of F_{arr} motors arrive at the tip per second, and that loss of motors is at a rate np_d for n motors at the tip, Q_n evolves according to the master equation

$$\frac{dQ_0}{dt} = p_d Q_1 - F_{arr} Q_0,$$

$$\frac{dQ_n}{dt} = F_{arr} Q_{n-1} + (n+1) p_d Q_{n+1} - F_{arr} Q_n - n p_d Q_n.$$

Solving for the steady (equilibrium) distribution $Q_n(t)=\tilde{Q}_n$ and normalizing so that $\Sigma_n Q_n=1$ gives the Poisson distribution

$$\tilde{Q}_n = \frac{\xi^n}{n!}\exp\,\xi \tag{16}$$

with parameter $\xi=F_{arr}/p_d$ as observed in simulations (see Fig. 5). The mean size of tip for this model is given by $\Sigma_n n\tilde{Q}_n$ which is precisely $\xi=F_{arr}/p_d$ in agreement with Eq. (15).

More generally, using Eq. (16) and $E[X(t)]=\Sigma_{n=0}^{\infty} nQ_n$, there is a closed form differential equation for $E[X(t)]$

$$\frac{d}{dt}\{E[X(t)]\} = F_{arr} - p_d E[X(t)]$$

with solution [for initial condition $X(0)=0$]

$$E[X(t)] = \frac{F_{arr}}{p_d}[1-\exp(-p_d t)]. \tag{17}$$

From the above Eq. (17), we can also see that starting from an empty tip, it will take a time approximately $O(\frac{1}{p_d})$ seconds for the tip size to approach the stationary state. This approximation of $E[X(t)]$ agrees well with simulations—Fig. 6 illustrates this, along with typical fluctuations of tip size for a single simulation.

More generally, the rate of slowest convergence to the equilibrium distribution of Eq. (16) (assuming rapidly decaying distributions) is $-p_d$, with corresponding eigenvector

$$R_n = \frac{\xi^n}{n!}(\xi - n).$$

Note that the eigenvector changes sign at the maximum of the distribution, the slowest decaying mode being associated with long-range fluctuations, and the rate coincides with the convergence rate in Eq. (17). As a consequence, transients in the mean size of the tip are expected to settle on a time scale of $1/p_d$. The agreement of the convergence rates suggests that, if this is a good model for the experiment of [15], then we expect fluctuations in tip size to settle on this time scale.

B. Other queueing models at tip

Further generalizations of this model could consider more complex queueing models such as those with nonmemoryless distributions of incoming and outgoing motors; queues with a finite number of "servers;" reducing the number of servers should not make a significant difference as long as the mean queue for each server is small. In addition, it would be interested to include a more realistic geometry for the queue, though it will still be a great challenge to discover the processes that governs the queue *in vivo*.

C. Conclusion

We have been able to present a model of a complete system of bidirectional motor transport using *in vivo* parameters and to predict the observed appearance of a fluctuating concentration of motors at the tip of a microtubule. In this paper we have focused on queueing effects induced by the exclusion dynamics of a stochastic transport model. We use a development of a model of Juhász [23] as a qualitative model of the bidirectional transport process observed in hyphal growth of *Ustilago maydis*.

The homogeneous stochastic model for motion on the MT predicts the dependence of the size of this concentration on

measurable transport parameters-the crucial parameters being the flux rate of arrival at the tip F_{arr} and the mean rate of turning of motors p_d—the latter can be obtained by estimating (as in [15]) the mean free path of motors away from the tip.

In principle, many predictions from the model, such as queuing properties, average densities and accumulation sizes can be experimentally measurable *in vivo*. In [15], the number of motors experimentally observed at the tip is in fact underestimated by this model by a factor of about two; the observed average number of dynein at the tip is approximately 55. The rate of turnover of the motors at the tip is also different in the experiment; the model here predicts that the turnover will be on the time scale $1/p_d$, while the experiment observes two populations in the queue; one with a fast turnover of order $1/p_d$, and one with a slower turnover; these observations suggests that there are (at least) two dynamical processes keeping dynein at the tip for [15] and the ASEP model discussed here is only one of these.

In fact, an additional control mechanism is been observed to capture a subpopulation of dynein at the plus-end in [15]; the capture mechanism involves plus-end binding proteins, such as EB1 and its interactor dynactin, that anchors the dynein complex to the MT tip [29]. Only a combination of the simple transport and the binding processes seem to be sufficient to explain the accumulation. We have not discussed the biological function of the accumulation, but recent work suggests that it ensures a high rate of capture of arriving organelles by preventing them from "falling off" the end of the track [15].

Our understanding of organelle transport is still at the beginning and this work is the first step toward a quantitative understanding of complex cellular transport mechanisms. Rapid progress in mathematical modeling and experimental research suggests a much more holistic understanding will be vital to understand complex cellular processes such as membrane trafficking in neurons.

ACKNOWLEDGMENT

We thank Martin Schuster for his assistance in the preparation of the experimental image used in Fig. 2.

[1] R. D. Vale, Cell **112**, 467 (2003).
[2] M. J. I. Muller, S. Klumpp, and R. Lipowsky, Proc. Natl. Acad. Sci. U.S.A. **105**, 4609 (2008).
[3] M. J. I. Muller, S. Klumpp, and R. Lipowsky, Biophys. J. **98**, 2610 (2010).
[4] M. A. Welte and S. P. Gross, HFSP J. **2**, 178 (2008).
[5] V. Soppina, A. K. Rai, A. J. Ramaiya, P. Barak and R. Mallik, Proc. Natl. Acad. Sci. U.S.A. **106**, 19381 (2009).
[6] Y. Okada, N. Higuchi, and N. Hirokawa, Nature **424**, 574 (2003).
[7] A. Seitz, H. Kojima, K. Oiwa, E. M. Mandelkow, Y. H. Song, and E. Mandelkow, EMBO J. **21**, 4896 (2002).
[8] R. J. McKenney, M. Vershinin, A. Kunwar, R. B. Vallee and S. P. Gross, Cell **141**, 304 (2010).
[9] Y. Chai, R. Lipowsky, and S. Klumpp, J. Stat. Phys. **135**, 241 (2009).
[10] I. A. Telley, P. Bieling, and T. Surrey, Biophys. J. **96**, 3341 (2009).
[11] J. R. Kardon, S. L. Reck-Peterson and R. D. Vale, Proc. Natl. Acad. Sci. U.S.A. **106**, 5669 (2009).
[12] H. M. Zhou, I. Brust-Mascher, and J. M. Scholey, J. Neurosci. **21**, 3749 (2001).
[13] S. Ma and R. L. Chisholm, J. Cell. Sci. **115**, 1453 (2002).
[14] D. Cai, K. J. Verhey, and E. Meyhoefer, Biophys. J. **92**, 4137 (2007).
[15] M. Schuster, S. Kilaru, P. Ashwin, C. Lin, N. J. Severs, and G. Steinberg (to be published).
[16] C. Arita, Phys. Rev. E **80**, 051119 (2009).
[17] T. Reichenbach, E. Frey, and T. Franosch, New J. Phys. **9**, 159 (2007).
[18] L. E. Hough, A. Schwabe, M. A. Glaser, J. R. McIntosh, and M. D. Betterton, Biophys. J. **96**, 3050 (2009).
[19] M. Ebbinghaus and L. Santen, J. Stat. Mech.: Theory Exp. (2009) P03030.
[20] M. Ebbinghaus, C. Appert-Rolland, and L. Santen, Phys. Rev. E **82**, 040901 (2010).
[21] M. Liu, K. Hawick, and S. Marsland, Phys. Lett. A **374**, 516 (2010).
[22] R. Juhász, Phys. Rev. E **76**, 021117 (2007).
[23] R. Juhász, J. Stat. Mech.: Theory Exp. (2010) P03010.
[24] A. Gennerich, A. P. Carter, S. L. Reck-Peterson, and R. D. Vale, Cell **131**, 952 (2007).
[25] D. T. Gillespie, J. Phys. Chem. **81**, 2340 (1977).
[26] M. J. I. Muller, S. Klumpp, and R. Lipowsky, J. Phys.: Condens. Matter **17**, S3839 (2005).
[27] D. Gross and C. M. Harris, *Fundamentals of Queueing Theory*, 2nd ed. (Wiley, Chichester, NY, 1985).
[28] P. Brémaud, *An Introduction to Probabilistic Modeling* (Springer, New York, 1988).
[29] A. Akhmanova and M. O. Steinmetz, Nat. Rev. Mol. Cell Biol. **9**, 309 (2008).